processes

MDPI

Article

Major Ion Geochemistry of Produced Water from Coalbed Methane Wells in the Gujiao Block and Its Relationship to Well Productivity

Gang Wang [1,2,*], Yong Qin [2], Liqiang Du [3], Yijia Yang [1] and Yan Li [1]

[1] College of Smart City Engineering, Shangqiu Normal University, Shangqiu 476000, China
[2] Key Laboratory of Coalbed Methane Resources and Reservoir Formation Process of the Ministry of Education, China University of Mining and Technology, Xuzhou 221116, China
[3] Shanxi Xi Shan Lan Yan Coalbed Methane Limited Liability Company, Taiyuan 030053, China
* Correspondence: wgkdwb@163.com

Abstract

To elucidate the geochemical features of produced water in coalbed methane (CBM) wells of the Gujiao Block and their indicative significance for production, systematic testing of ion composition and total dissolved solids (TDS) of produced water from ten CBM wells was conducted through five discrete sampling campaigns over an 18-month period. Combined with production performance data, the spatiotemporal evolution patterns, controlling factors, and the response relationship with productivity were analyzed. The results show that the water chemistry type of produced water in the study area is mainly identified as the Na-HCO_3 type. The TDS averages 1716.62 mg/L. The hydrochemical characteristics are primarily controlled by water/rock interactions, with Na^+ and K^+ mainly derived from silicate mineral weathering and dissolution, coupled with cation exchange processes. The Na/Cl ratio suggests that halite dissolution contributes to both Na^+ and Cl^-, whereas the excess Na^+ relative to Cl^- likely reflects cation exchange or dissolution of Na-bearing silicate minerals. As drainage proceeded, Na^+ and K^+ concentrations increased, Ca^{2+} decreased, Cl^- increased, and $SO_4{}^{2-}$ first increased and then decreased. Spatially, TDS increases from north to south, with the central-southern region representing a stagnant groundwater zone. Productivity response analysis reveals that Na^+, $HCO_3{}^-$, and TDS all show a trend of initially slow increase followed by rapid increase with increasing gas production. A negative trend is observed between gas production and the concentrations of Cl^-, Ca^{2+}, Mg^{2+}, and $SO_4{}^{2-}$. The productivity response index for the Gujiao Block ranges from 3.75 to 42.43, with an average of 17.78. As the productivity response index increases, gas production initially decreases and then increases. The findings clarify the geochemical evolution mechanisms of produced water in the Gujiao Block, providing a scientific basis for productivity evaluation of CBM wells.

Keywords: produced water; major ion geochemistry; coalbed methane; Gujiao Block; productivity response; hydrogeochemistry

Check for updates

Academic Editor: Tianshou Ma

Received: 13 June 2026
Revised: 24 July 2026
Accepted: 28 July 2026
Published: 30 July 2026

Copyright: © 2026 by the authors. Licensee MDPI, Basel, Switzerland. This article is an open access article distributed under the terms and conditions of the Creative Commons Attribution (CC BY) license.

1. Introduction

As a clean and efficient unconventional natural gas resource, the development and utilization of coalbed methane (CBM) are of great significance for alleviating energy shortages and optimizing energy structures [1]. The hydrogeochemical characteristics of produced

water (also referred to as drainage water) from CBM wells contain a wealth of information regarding reservoir geology and production performance. They can not only reveal the hydrochemical evolution patterns of coal reservoirs but also effectively indicate CBM productivity potential, thereby providing a scientific basis for optimizing production layer combinations and the strategies used for drainage [2–5]. For instance, studies in the Qinshui Basin's Zhengzhuang Block have confirmed that changes in total dissolved solids (TDS) and major ion concentrations in produced water during the stable drainage stage exhibit a significant response relationship with high CBM production [6]. In the southern Qinshui Basin CBM field, the produced water is largely of the Na-HCO_3 type, and its hydrogen and oxygen isotopic characteristics reveal the pressure-maintaining and enrichment effect of atmospheric precipitation on CBM occurrence, further highlighting the importance of produced water geochemistry in understanding CBM accumulation and development [7].

Recently, numerous studies have been conducted on the geochemical features and productivity indication of water discharged from CBM wells, yielding a variety of insights. Regarding the hydrochemical types and controlling factors of produced water, both commonalities and differences exist among different blocks. The Panhe Block and the Fanzhuang Block are located in the southern part of the Qinshui Basin. In the Panhe Block, the produced water is mainly of the Na-HCO_3 type and weakly alkaline. Its chemical characteristics are mainly controlled by cation exchange adsorption and desulfidation—two core water–rock interaction processes [2]. Studies in the Fanzhuang Block indicate that both original TDS and drainage flow rate jointly influence the intensity of water/rock reactions; stronger water/rock interactions occur under conditions of higher TDS and lower flow rates. $Na^+ + K^+$ and Cl^- concentrations rise with increasing TDS. In addition, there exist certain ranges of TDS and flow rate that favor the dissolution of Ca^{2+} and Mg^{2+} [8]. In the Zhijin Block of western Guizhou, the produced water's trace element concentrations are controlled by water–coal interactions, with soluble elements being extensively leached under stagnant conditions, and trace element concentrations are closely related to groundwater hydrodynamic conditions [9]. The produced water in the Junlian Block of Sichuan exhibits characteristics of "high TDS, high Cl^-, high SO_4^{2-}, and low HCO_3^-". Hydrogen and oxygen isotopic compositions and ionic compositions reveal a mixing process between infiltrating atmospheric precipitation and marine original formation water. Wells in the synclinal axis have better sealing conditions, favorable CBM preservation, and higher productivity potential [10].

Many investigations have documented that key geochemical parameters of produced water can effectively indicate coalbed methane well productivity. In the Fanzhuang Block, the Ca^{2+} concentration in produced water from the No. 3 coal seam presents a notable positive correlation with gas production. It is also worth noting that the response mechanism of Ca^{2+} varies noticeably under different water and gas drainage modes. The high water production–moderate gas production mode is governed chiefly by water–rock reactions taking place in the sandstone aquifer of the floor, whereas the low water production–high gas production mode is related to calcite dissolution within the coal seam [8]. In the Zhijin Block of western Guizhou, the Li concentration in produced water is positively correlated with average daily gas production, and the spider diagram area of characteristic trace element concentrations is negatively correlated with average daily water production, effectively suggesting hydrodynamic conditions and productivity potential [9]. In the Zhengzhuang Block of the Qinshui Basin during the stable drainage stage, Ca^{2+} content in high-productivity areas rises with the gas/water ratio, while Cl^- content falls as this ratio increases. A high-productivity response model based on calcite dissolution and organic complex formation has been established [6]. Furthermore, studies in blocks such as the Santang Syncline in western Guizhou and the Fukang Mining Area have also focused

on the influence of produced water sources (e.g., coal-measure stagnant water, overlying aquifer water, fracturing fluid flowback) on the drainage process, proposing targeted post-fracturing flowback and drainage control measures [11,12].

Existing studies have elucidated various aspects of the produced water geochemistry. However, research on the Gujiao Block remains significantly insufficient. Current studies are mostly concentrated in mature development blocks such as the Zhengzhuang, Panhe, and Fanzhuang blocks of the Qinshui Basin, the Zhijin and Santang Syncline blocks of western Guizhou, and the Junlian Block of Sichuan [2,6,8,9,12]. In contrast, the Gujiao Block, as an important part of North China's CBM resources, has not yet undergone systematic geochemical research on produced water. Its hydrochemical types, controlling factors, and productivity indication patterns remain unclear, and the research findings from other blocks cannot be directly applied. The Gujiao Block is a significant CBM development area in China, characterized by complex geological conditions and abundant CBM resources. In-depth investigation of the major ion geochemical features of produced water in the Gujiao Block can help reveal the enrichment patterns and development mechanisms of CBM in this region. It should be emphasized that the relationships between ion concentrations and gas production observed in this study are correlative rather than causal. Gas production is influenced by multiple factors beyond water chemistry, including reservoir pressure, permeability, coal structure, drainage strategy, well completion, and production history. The geochemical analysis presented here provides one line of evidence for productivity assessment. In this study, we focus on major ions (Na^+, K^+, Ca^{2+}, Mg^{2+}, HCO_3^-, Cl^-, SO_4^{2-}) rather than trace elements or isotopes, because major ions are routinely measured at low cost and have been widely used in CBM productivity studies in other Qinshui Basin blocks, enabling direct comparison with previous work.

2. Geological Setting

The Gujiao Block is situated in the northwestern Qinshui Basin of China's Shanxi Province, sitting to the west of Taiyuan City. The overall structure within the block is relatively complex. Notably, it is primarily characterized by a series of northeast-trending faults and synclines that trend approximately north to south. The primary coal-bearing formations are dominated by two key units. Specifically, these are the Shanxi Formation and the Taiyuan Formation. At present, the coal seams targeted for coalbed methane (CBM) well production are concentrated in two key formations. Specifically, these include the No. 2 coal seam in the Shanxi Formation, along with the No. 8 and No. 9 coal seams in the Taiyuan Formation. The No. 2 coal seam of the Shanxi Formation occurs at depths of approximately 270.48–818.70 m, with an average thickness of 1.63 m; the No. 8 and No. 9 coal seams of the Taiyuan Formation occur at 357.01–915.15 m, with average thicknesses of 2.61 m and 2.54 m, respectively. Permeability of these coal seams ranges from 0.016 to 0.060 mD. In the northern part of the study area, the gas content is relatively low, generally below 4 m^3/t. In contrast, the highest gas content occurs in the Xingjiashe mine field in the southern part, reaching approximately 20 m^3/t. Reservoir pressure gradients are generally 0.41–0.95 MPa/100 m, indicating slightly underpressured to normal conditions [13]. The groundwater in this area is recharged by atmospheric precipitation in the northern and northwestern parts of the Xishan Coalfield. Influenced by the Malan Syncline, it converges southward and toward the synclinal axis. The sandstone and limestone intervals within the Shanxi and Taiyuan formations constitute the principal aquifers [13].

Most CBM wells in the broader Gujiao Block reportedly have long-term average gas production rates below approximately 200 m^3/d [14], although several wells included in the present data set show substantially higher production rates at individual sampling times. The productivity of CBM wells in this region is influenced by multiple factors, among

which structural and hydrogeological conditions are the primary geological controlling factors [14]. In-depth investigation of the major ion geochemical characteristics of produced water from CBM wells in this block and its indication for productivity can help reveal the CBM enrichment patterns in this area and provide a basis for further rational development.

3. Materials and Methods

A total of 18 months of sampling was conducted in this study. The first four sampling events were carried out at intervals of three months, with a six-month interval between the fourth and fifth samplings. Due to the variation in production layers among different coalbed methane (CBM) wells, wells with commingled production from the No. 2, No. 8, and No. 9 coal seams were primarily selected; MCQ4 produces solely from the No. 8 coal seam, MCQ2 uses commingled mining of No. 8 and No. 9 coal seams, and all remaining wells adopt combined extraction of No. 2, No. 8 and No. 9 coal seams. Sampling took place at each CBM wellhead—locations are given in Reference [13]. Water samples were collected directly from the wellhead after flow conditions had stabilized. The samples were not filtered or acidified in the field and were immediately sealed in pre-cleaned polyethylene bottles before transportation to the laboratory. The samples were then promptly dispatched to the Institute of Geochemistry, Chinese Academy of Sciences (Guiyang), for analysis. Among the anions, HCO_3^- was determined by acid titration, and other anions were assessed with ion chromatography using a Dionex (Thermo Fisher, USA) ICS-90 system equipped with an AG14-AS14 column (4 × 250 mm). Detection was performed using a self-regenerating suppressed conductivity detector. The detection limit for all anions was 0.1 mg/L. As for the cations, they were measured by inductively coupled plasma optical emission spectrometry (ICP-OES) using a Varian Vista MPX instrument (USA), with detection limits ranging from ppb to ppm levels depending on the element. Before ICP-OES measurement, the samples were filtered in the laboratory; therefore, the reported cation concentrations represent dissolved concentrations. A summary of the detailed results is provided in Table 1. Most wells are produced from commingled seams (No. 2, No. 8, and No. 9), so the produced water represents a mixture from different coal seams and possibly adjacent aquifers. Therefore, the geochemical signatures reflect bulk mixing rather than conditions of individual seams.

Field measurements of pH, Eh, and electrical conductivity (EC) were recorded at the time of sampling. The pH values ranged from 7.7 to 9.8 (average 8.5), indicating weakly to moderately alkaline conditions. Eh values ranged from −878 to 209 mV (average −188 mV), suggesting generally reducing conditions. EC ranged from 297 to 3500 μS/cm (average 2490 μS/cm). Because the samples were neither filtered nor acidified in the field, the possibility of precipitation, particularly Ca^{2+} and Mg^{2+}, during transportation cannot be entirely ruled out.

All statistical analyses were performed using SPSS Statistics 25.0. Pearson correlation coefficients were calculated to evaluate linear relationships among ion concentrations, TDS and drainage days. Two-tailed significance tests were conducted, with $p < 0.05$ considered statistically significant and $p < 0.01$ considered highly significant. Missing data (denoted by "/" in tables) were excluded pairwise; no imputation was applied. The number of valid sample pairs ($n = 44$) was consistent across all correlation calculations, as all ion measurements were available for 44 samples. Regression analysis was not performed for the productivity–ion relationships due to the exploratory nature of this study; instead, trends are supported by correlation coefficients and p-values. All correlations presented in this study are exploratory and may reflect differences among wells, as well as temporal changes within individual wells.

Table 1. Ion concentrations of produced water (unit: mg/L).

Well	Drainage Days (d)	Sampling Frequency	Ca^{2+}	K^+	Mg^{2+}	Na^+	F^-	Cl^-	NO_3^-	SO_4^{2-}	Br^-	HCO_3^-	TDS
MCQ1	214	1	2.23	1.41	1.41	19.44	1.20	193.49	/	0.26	1.52	1683.31	1062.62
	304	2	16.13	5.43	8.01	648.47	1.12	202.12	/	0.08	1.59	1720.99	1743.44
	395	3	/	/	/	/	/	/	/	/	/	/	/
	518	4	13.21	6.36	3.91	725.60	1.29	234.37	0.16	0.35	1.49	1730.60	1851.88
	730	5	14.08	6.99	3.50	1087.70	1.40	224.80	/	0.15	1.44	1744.80	2212.47
MCQ2	364	1	8.92	4.33	4.18	851.38	2.64	171.41	/	8.17	1.10	2160.66	2132.46
	454	2	5.41	5.30	4.26	756.33	3.05	178.90	/	1.95	1.18	2102.04	2007.40
	545	3	4.88	7.14	2.51	930.10	2.66	178.57	/	0.76	1.20	2171.60	2213.62
	668	4	6.22	6.95	2.23	848.68	2.80	172.09	0.24	1.49	1.13	2181.20	2132.18
	880	5	/	/	/	/	/	/	/	/	/	/	/
MCQ3	364	1	5.51	2.52	3.10	693.71	1.09	135.92	/	0.51	1.24	1930.36	1808.77
	454	2	9.10	5.42	5.39	761.79	1.32	161.49	/	2.10	0.78	2164.85	2029.82
	545	3	5.53	5.21	2.31	790.60	1.10	138.09	/	0.35	1.23	1922.40	1905.63
	668	4	8.63	5.13	1.88	765.21	1.17	138.83	/	1.16	1.29	1927.10	1886.85
	880	5	7.32	5.43	1.75	1082.20	1.32	134.96	0.11	0.53	1.39	1870.30	2170.04
MCQ4	406	1	3.67	0.34	1.58	689.64	4.38	105.27	/	7.66	0.56	1700.06	1663.13
	496	2	5.81	2.55	3.09	747.78	4.74	109.70	/	7.51	0.48	1666.56	1714.94
	587	3	3.52	3.22	1.54	706.00	4.55	108.92	/	3.82	0.68	1735.40	1699.96
	710	4	4.18	2.91	1.66	708.39	4.38	116.51	/	4.16	0.54	1620.30	1652.88
	922	5	3.58	3.43	1.24	1003.50	4.60	104.60	0.26	6.71	0.43	1744.80	2000.50
MCQ5	544	1	10.69	2.07	6.44	789.93	2.84	98.97	/	0.27	1.15	2085.29	1955.01
	634	2	12.11	4.44	7.87	717.72	3.02	103.23	/	0.54	1.39	2102.04	1901.33
	725	3	8.16	4.98	4.13	774.50	2.82	92.75	/	1.14	1.38	2008.60	1894.16
	848	4	11.76	4.88	3.96	889.96	2.80	104.93	0.22	0.39	1.25	2061.40	2050.63
	1060	5	/	/	/	/	/	/	/	/	/	/	/
MCQ6	358	1	4.45	3.24	1.67	702.40	3.80	49.53	/	1.75	0.46	1825.68	1680.14
	448	2	5.24	3.69	2.80	713.44	3.94	51.44	/	1.93	0.52	1754.49	1660.26
	539	3	3.17	4.82	1.44	696.10	3.89	55.52	/	0.82	0.62	1836.10	1684.42
	662	4	3.58	4.49	1.60	828.06	3.68	82.52	0.12	1.03	0.49	1759.40	1805.15
	874	5	2.63	5.12	1.25	1033.50	4.02	57.72	/	0.18	0.50	1744.00	1976.93
MCQ7	878	1	6.63	2.39	8.49	802.89	0.79	320.62	/	2.83	3.25	1679.12	1987.44
	968	2	8.55	5.07	8.63	681.68	1.05	338.95	/	0.72	3.28	1666.56	1881.21
	1059	3	9.04	6.32	5.63	856.80	1.06	391.62	/	0.39	3.76	1746.90	2148.07
	1182	4	5.17	5.90	4.64	870.02	1.06	391.95	/	1.96	3.68	1735.40	2152.08
	1394	5	4.54	7.58	3.96	1248.80	1.09	386.75	0.20	0.41	3.76	1725.20	2519.49
MCQ8	385	1	5.50	0.18	0.97	491.82	6.27	104.95	/	26.47	0.38	1214.33	1243.70
	475	2	7.13	2.23	2.25	431.91	6.25	107.43	/	24.62	0.22	1226.89	1195.49
	566	3	6.67	2.66	1.20	513.00	6.45	107.50	/	15.60	0.43	1212.90	1259.96
	689	4	5.82	2.25	1.22	531.31	6.39	107.61	0.27	12.16	0.30	1227.20	1280.65
	901	5	/	/	/	/	/	/	/	/	/	/	/
MCQ9	378	1	/	/	/	/	/	/	/	/	/	/	/
	468	2	4.74	0.69	1.62	177.44	8.52	151.76	/	11.47	0.68	460.61	587.21
	559	3	4.84	1.39	0.97	258.50	8.55	155.20	/	11.28	0.69	479.40	681.12
	682	4	4.32	0.93	0.87	283.60	7.95	168.25	0.21	11.76	0.63	1620.30	1288.47
	894	5	4.13	1.44	0.83	408.36	7.57	172.87	/	16.39	0.58	411.70	818.02
MCQ10	241	1	10.90	1.17	3.74	563.56	3.63	68.59	/	0.48	0.65	1637.25	1471.35
	331	2	12.69	2.61	5.16	496.52	3.64	71.20	/	0.35	0.79	1599.56	1392.75
	422	3	10.66	3.88	2.92	630.90	3.50	69.01	/	0.24	0.78	1641.40	1542.59
	545	4	9.62	2.98	2.17	681.69	3.72	68.87	/	0.31	0.96	1629.90	1585.27

Note: "/" indicates no data.

4. Geochemical Characteristics

4.1. Ion Concentration Analysis

All missing data were excluded before averaging, and each valid sample was weighted equally when calculating mean ion concentrations and TDS. TDS was calculated as the sum of all measured ion mass concentrations, with one-half of the HCO_3^- concentration included in the summation. The total dissolved solids (TDS) of the produced water from CBM wells in the study area range from 818.02 to 2519.49 mg/L, with an average value of 1716.62 mg/L. The dominant cations are Ca^{2+}, Na^+, K^+, and Mg^{2+}, while the domi-

nant anions are HCO_3^-, Cl^-, and SO_4^{2-}. Among these, the concentrations of Na^+, Cl^-, and HCO_3^- are relatively high, with average values of 702.07 mg/L, 152.04 mg/L, and 1680.24 mg/L, respectively. The concentrations of Ca^{2+}, K^+, Mg^{2+}, and SO_4^{2-} are relatively low, averaging 7.06 mg/L, 3.81 mg/L, 3.18 mg/L, and 4.39 mg/L, respectively. Other ions, such as F^-, Br^-, and NO_3^-, are also present at low concentrations (Table 1).

The relationships among various ions in the produced water exhibit diversity. A correlation coefficient ($|r|$) less than 0.5 indicates poor correlation; $0.5 < |r| < 0.7$ indicates moderate correlation; and $|r| > 0.7$ indicates good correlation. Except for F^- and SO_4^{2-}, all other ions show positive correlations with TDS. Among these, K^+ (r = 0.79), Na^+ (r = 0.92), and HCO_3^- (r = 0.84) display good positive correlations, while Br^- shows a moderate correlation. The high concentrations of Na^+ and HCO_3^- make them the primary contributors to TDS in the water. HCO_3^- exhibits a variation trend consistent with TDS, shows negative correlations with F^- (r = −0.73) and SO_4^{2-} (r = −0.65), moderate positive correlations with K^+ and Na^+, and poor correlations with other ions. Br^- has a good correlation with Cl^- (r = 0.90), moderate correlations with K^+ and Mg^{2+}, and a negative correlation with F^-. F^- shows moderate correlations with K^+, Mg^{2+}, and Na^+. SO_4^{2-} has a good correlation with F^- (r = 0.74) and a moderate correlation with K^+. Na^+ and K^+ exhibit a good positive correlation with a correlation coefficient of 0.74. This close relationship suggests that Na^+ and K^+ may originate from similar geological sources, possibly derived primarily from the weathering and dissolution of silicate minerals such as albite and potassium feldspar, or from cation exchange processes in the aquifer [15]. Meanwhile, the correlation between Ca^{2+} and Mg^{2+} (r = 0.63) is moderately good (Table 2; Figure 1).

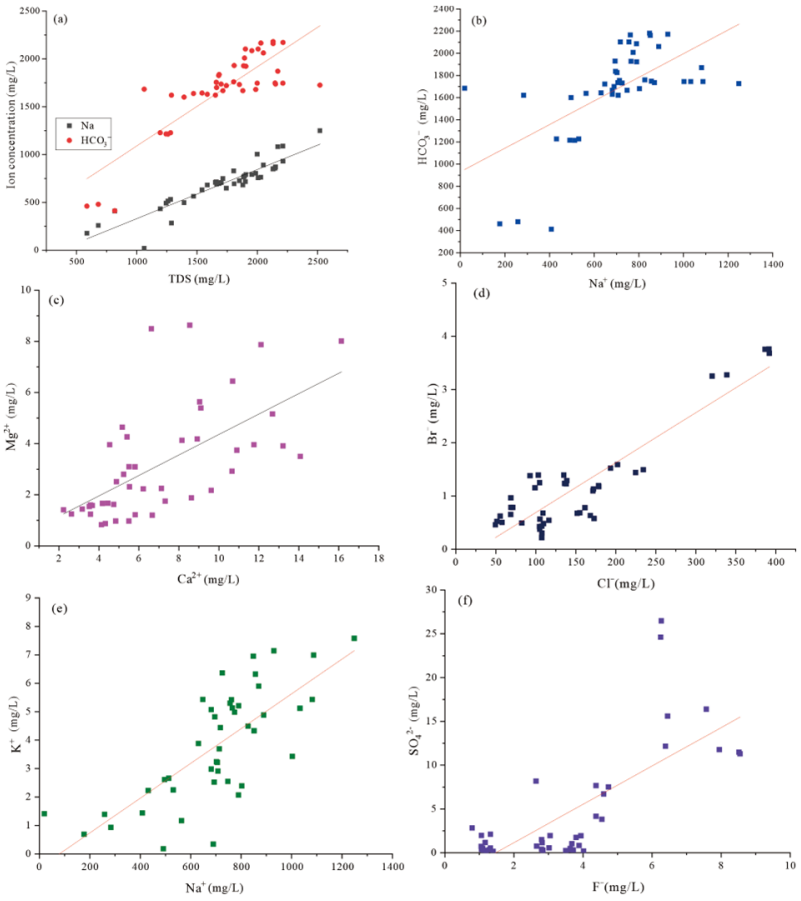


Figure 1. Scatter diagram for the correlation analysis of ion concentrations. Panels (**a**–**f**) show pairwise scatter plots for selected ion pairs: (**a**) Na^+ and HCO_3^- vs. TDS; (**b**) HCO_3^- vs. Na^+; (**c**) Mg^{2+} vs. Ca^{2+}; (**d**) Br^- vs. Cl^-; (**e**) K^+ vs. Na^+; (**f**) SO_4^{2-} vs. F^-.

Table 2. Pearson correlation coefficients (*r*) among ions and drainage days.

Correlation	Ca^{2+}	K^+	Mg^{2+}	Na^+	F^-	Cl^-	SO_4^{2-}	Br^-	HCO_3^-	TDS	Drainage Days
Ca2+	1	0.28	0.63 **	0.15	−0.37 *	0.08	−0.28	0.18	0.23	0.22	−0.16
K+		1	0.32 *	0.74 **	−0.67 **	0.42 **	−0.59 **	0.50 **	0.58 **	0.79 **	0.45 **
Mg2+			1	0.25	−0.58 **	0.47 **	−0.42 **	0.62 **	0.38*	0.43 **	0.14
Na+				1	−0.58 **	0.22	−0.49 **	0.37 *	0.62 **	0.92 **	0.54 **
F−					1	−0.44 **	0.74 **	−0.64 **	−0.73 **	−0.78 **	−0.18
Cl−						1	–0.14	0.90 **	0.01	0.35*	0.61 **
SO42−							1	−0.40 **	−0.65 **	−0.61 **	−0.12
Br−								1	0.22	0.51 **	0.63 **
HCO3−									1	0.84 **	−0.01
TDS										1	0.43 **
Drainage days											1

Note: ** $p < 0.01$ (two-tailed); * $p < 0.05$ (two-tailed).

The Gibbs diagram utilizes the equilibrium relationships among ions and molecules in water to analyze the sources and evolution processes of dissolved constituents and is widely employed in studies of groundwater chemical interaction mechanisms [16]. Ion concentrations in the diagram are expressed in meq/L units [15]. In Figure 2a, the data points do not fall within any defined mechanism domain. Figure 2b shows that the samples plot close to or within the water/rock interaction zone, and are relatively distant from the evaporation/crystallization domain, indicating that the produced water is primarily influenced by water/rock interactions. However, the Gibbs diagram alone provides only a preliminary indication. To further constrain the controlling mechanisms, we examine multiple ion ratio relationships—including Na^+/Cl^- and $(Ca^{2+} + Mg^{2+})/(HCO_3^- + SO_4^{2-})$—in the following section.

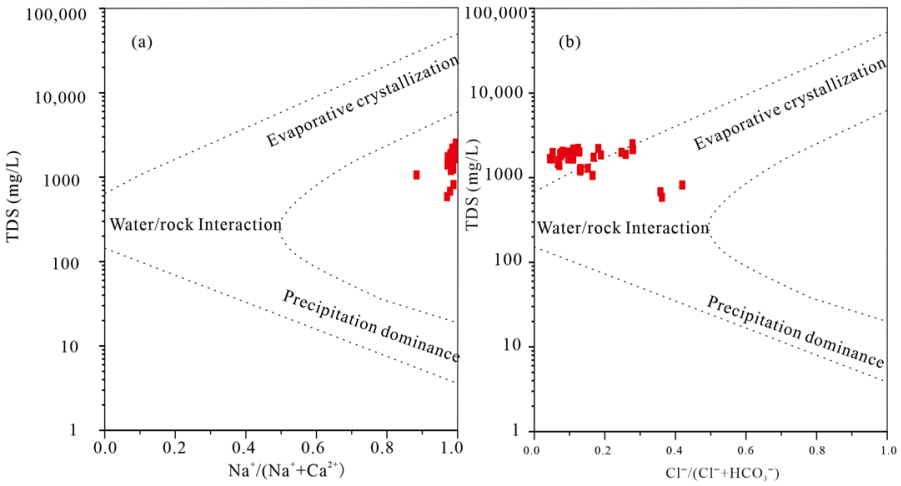


Figure 2. Gibbs diagram of produced water chemistry (ion concentrations in meq/L). (**a**) $Na^+/(Na^+ + Ca^{2+})$ vs. TDS; (**b**) $Cl^-/(Cl^- + HCO_3^-)$ vs. TDS.

A Na/Cl ratio of 1:1 indicates that these ions originate from halite dissolution. The majority of samples from the study area plot on or above the 1:1 line of Na^+ versus Cl^-, suggesting that, in addition to halite dissolution, excess Na+ relative to CI may reflect cation exchange or dissolution of Na-bearing silicate minerals [17]. If Ca^{2+} and Mg^{2+} were derived solely from carbonate dissolution, the $(Ca^{2+} + Mg^{2+})/(HCO_3^- + SO_4^{2-})$ molar ratio would be 1:1. The water samples all plot below the 1:2 line, indicating a deficit in Ca^{2+} and Mg^{2+} concentrations, likely due to carbonate precipitation [17] (Figure 3).

Ion ratio coefficients can be used to analyze the formation mechanisms of groundwater. The $Br^- \times 10^3/Cl^-$ ratio in seawater is 3.4. Groundwater with a value lower than this is classified as leachate water, while that with a value higher than this is classified as primary sedimentary brine [18]. Statistical analysis shows that the values for wells MCQ3, MCQ5,

MCQ6, MCQ7, and MCQ10 in the produced water are greater than 3.4, suggesting that the water from these wells may be primary sedimentary brine. For the remaining wells, except for well MCQ1, which fluctuates around 3.4, all others have values lower than 3.4, indicating that these wells likely produce mainly leachate water (Figure 4). However, this classification is only qualitative; Br^-/Cl^- ratios can also be affected by halite dissolution, mixing with different water masses, evaporation, and analytical uncertainty. Therefore, Br^-/Cl^- ratios should be interpreted together with Cl^- concentration, TDS, and the regional hydrogeological setting. According to a study by Gu et al. [10], as atmospheric precipitation infiltrates, the sealing performance of CBM wells deteriorates, and conventional ions exhibit regular variations. In the Gujiao Block, wells closer to the recharge zone of precipitation yield water that tends to be leachate in character, while those farther from the recharge zone or in stagnant groundwater areas yield water that tends to be primary sedimentary brine.

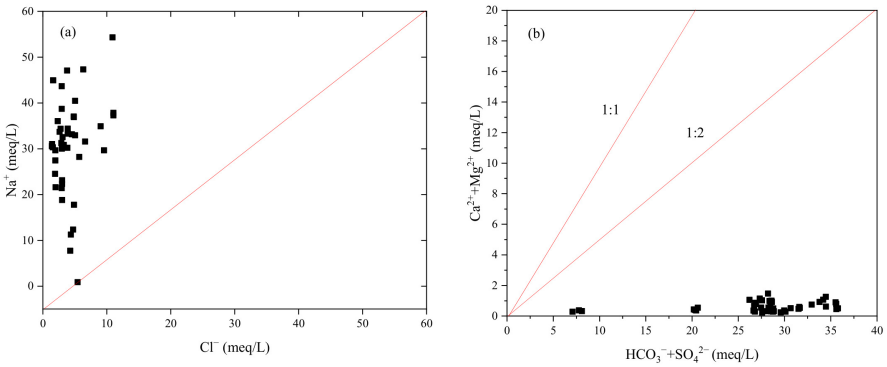


Figure 3. Ion ratio relationships. (**a**) Na^+ vs. Cl^- (meq/L); (**b**) (Ca^{2+} + Mg^{2+}) vs. (HCO_3^- + SO_4^{2-}) (meq/L).

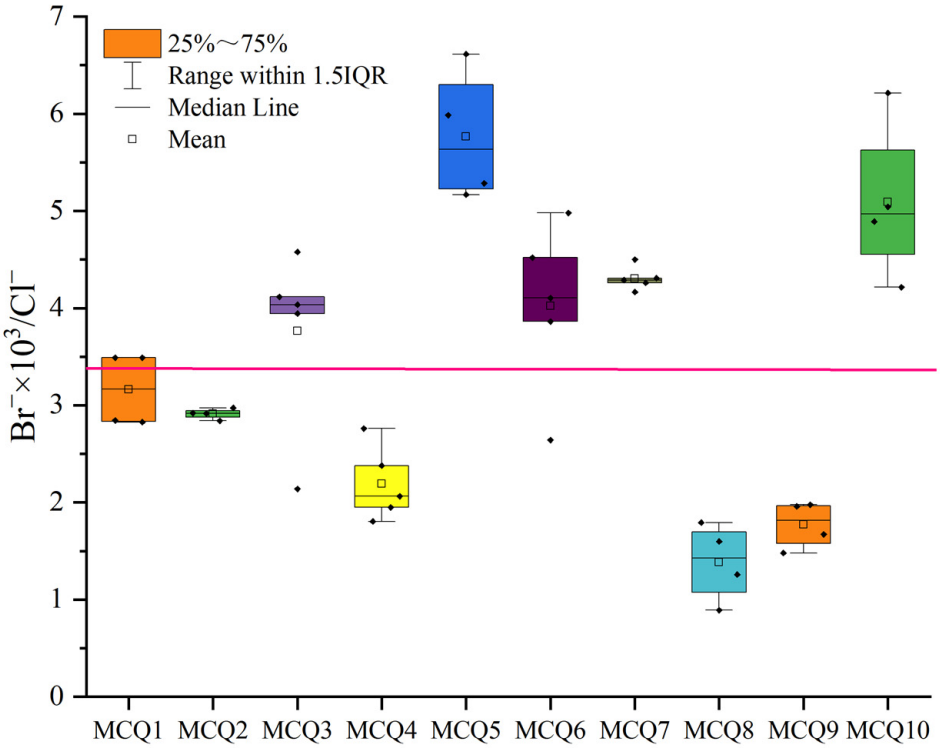


Figure 4. Comparison of $Br^- \times 10^3/Cl^-$ ratios in different CBM wells (the horizontal line at 3.4 indicates the seawater ratio for Reference [18]).

4.2. Temporal Variation Patterns

The water samples were grouped according to drainage time. The results show that within the first year of drainage (214–364 days), the predominant cation in the samples is Na^+, with concentrations varying from 19.44 to 851.38 mg/L (average 567.93 mg/L), followed by Ca^{2+}. The predominant anion is HCO_3^- (average 1793.97 mg/L), followed by Cl^- (average 127.47 mg/L), while other ions are present at relatively low concentrations. The TDS varies from 1062.62 to 2132.46 mg/L, with an average concentration of 1613.07 mg/L. For drainage durations between 378 and 730 days, Na^+ remains the predominant cation, varying from 177.44 to 1087.70 mg/L (average 668.06 mg/L), followed by Ca^{2+}. HCO_3^- is still the dominant anion (average 1663.92 mg/L), with Cl^- as the secondary anion (average 125.65 mg/L). TDS varies from 587.21 to2213.62 mg/L (average 1649.47 mg/L). For drainage durations between 848 and 1394 days, Na^+ remains the dominant cation (408.36–1248.80 mg/L, average 887.77 mg/L), followed by Ca^{2+}. HCO_3^- continues to be the dominant anion (411.70–2061.40 mg/L, average 1644.71 mg/L), with Cl^- averaging 240.50 mg/L. TDS varies from 818.02 to 2519.49 mg/L (average 1970.44 mg/L).

Across the pooled drainage time groups, the mean Na^+ and K^+ concentrations are higher in the latter group, whereas the mean Ca^{2+} concentration is lower. However, because the groups contain different wells and unequal sample numbers, these differences cannot be attributed solely to temporal evolution during drainage (Table 3, Figure 5). The Piper diagram offers an effective way to investigate the chemical composition and water types of groundwater. In the Piper diagram, all produced water samples from the study area fall within zone II, indicating a Na-HCO_3 water type. This water type is similar to that observed in the Zhengzhuang Block of the Qinshui Basin. This indicates that the water originates from deep strata or coal seam water and is minimally influenced by surface water or shallow groundwater [6] (Figure 6).

Table 3. Statistical data for different drainage stages.

Drainage Days (d)	Number of Samples		Ca^{2+}	K^+	Mg^{2+}	Na^+	F^-	Cl^-	SO_4^{2-}	Br^-	HCO_3^-	TDS
214–364	7	min	2.23	1.17	1.41	19.44	1.09	49.53	0.08	0.46	1599.56	1062.62
		max	16.13	5.43	8.01	851.38	3.80	202.12	8.17	1.59	2160.66	2132.46
		average	8.69	2.96	3.90	567.93	2.45	127.47	1.66	1.05	1793.97	1613.07
378–730	27	min	3.17	0.18	0.87	177.44	1.10	51.44	0.15	0.22	460.61	587.21
		max	14.08	7.14	7.87	1087.70	8.55	234.37	26.47	1.49	2181.20	2213.62
		average	6.91	3.67	2.68	668.06	4.10	125.65	5.60	0.84	1663.92	1649.47
848–1394	10	min	2.63	1.44	0.83	408.36	0.79	57.72	0.18	0.43	411.70	818.02
		max	11.76	7.58	8.63	1248.80	7.57	391.95	16.39	3.76	2061.40	2519.49
		average	6.34	4.76	4.04	887.77	2.54	240.50	3.05	2.19	1644.71	1970.44

The average TDS shows a gradual increasing trend with drainage time. However, the proportions of individual components exhibit certain temporal patterns. As drainage proceeds, the concentration ratios of Na^+ and K^+ gradually increase. During the 214–364 day stage, the average proportions of Na^+ and K^+ are 21.68% and 0.11%, respectively; during the 378–730 day stage, these average proportions are 26.69% and 0.14%; and during the 848–1394 day stage, they reach 32.24% and 0.17%, respectively. Cl^- also increases from 5.19% to 9.15%. The proportion of HCO_3^- decreases from 72.31% to 57.64%, while the proportion of Ca^{2+} gradually declines from 0.35% to 0.24%. The proportions of Mg^{2+}, F^-, SO_4^{2-}, and Br^- exhibit fluctuating variations (Table 4).

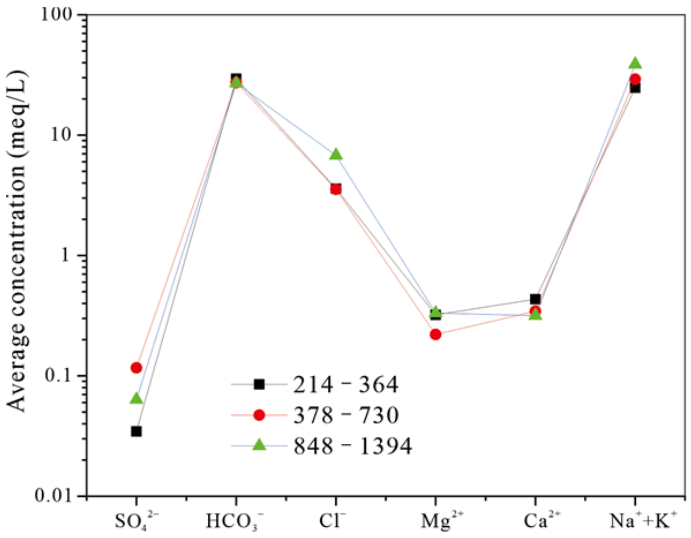


Figure 5. Schoeller diagram of produced water chemistry.

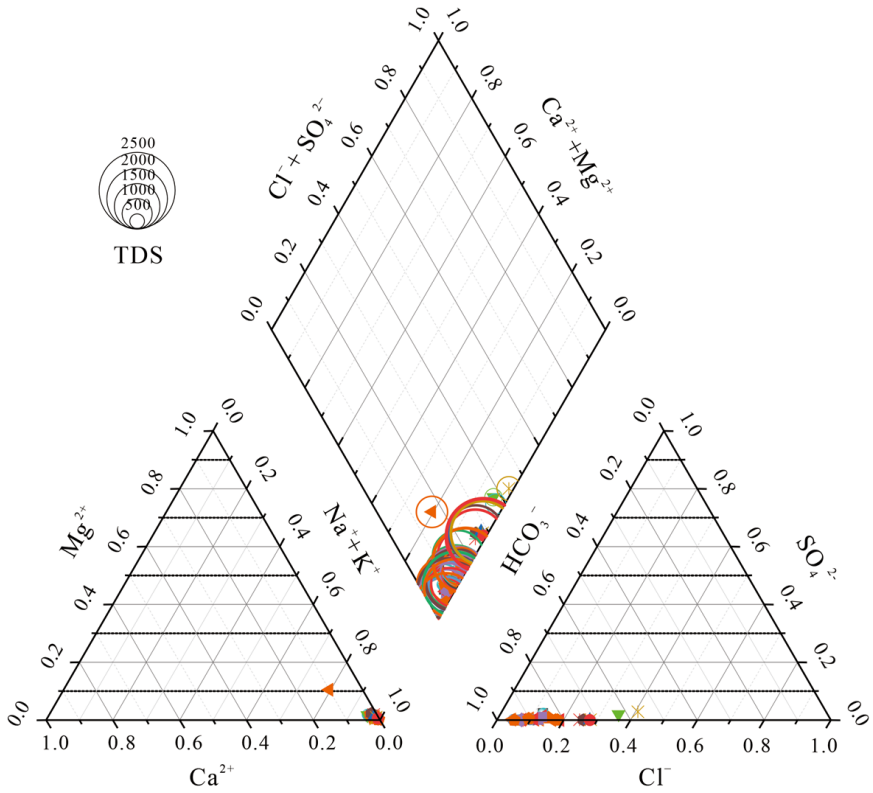


Figure 6. Piper diagram of produced water chemistry (values in milliequivalent percentages).

Table 4. Average proportions of ions at different stages (calculated as mass concentration percentages).

Drainage Days (d)	Na^+	Ca^{2+}	Mg^{2+}	K^+	F^-	Cl^-	SO_4^{2-}	Br^-	HCO_3^-
214–364	21.68	0.35	0.16	0.11	0.10	5.19	0.06	0.04	72.31
378–730	26.69	0.29	0.11	0.14	0.22	5.72	0.33	0.03	66.46
848–1394	32.24	0.24	0.14	0.17	0.13	9.15	0.21	0.08	57.64

4.3. Spatial Variation Patterns

The TDS contour maps were generated using ordinary kriging interpolation, implemented in Surfer 8.0 software with default software settings. Each panel was constructed

using the available well data for each sampling event: 10 wells for the second and fourth samplings, and 9 wells for the first and third samplings (MCQ1 had no third-round data; MCQ9 had no first-round data). Missing values were not estimated; interpolation was based only on available well data. Because of the limited number of wells, interpolation uncertainty is inherently high; the maps are intended to illustrate the general spatial trend of TDS variation rather than a high-precision quantitative distribution. Spatially, the overall TDS trend shows a consistent pattern of gradual increase from north to south, which is consistent with the regional structural configuration: the coal seam floor elevation shows a north-to-south decreasing trend [13]. The central-southern part shows relatively high TDS, consistent with the previously proposed low-flow or relatively stagnant hydrogeological setting [13]. Although the TDS center shifts slightly over time, the overall change is relatively minor across the study area (Figure 7).

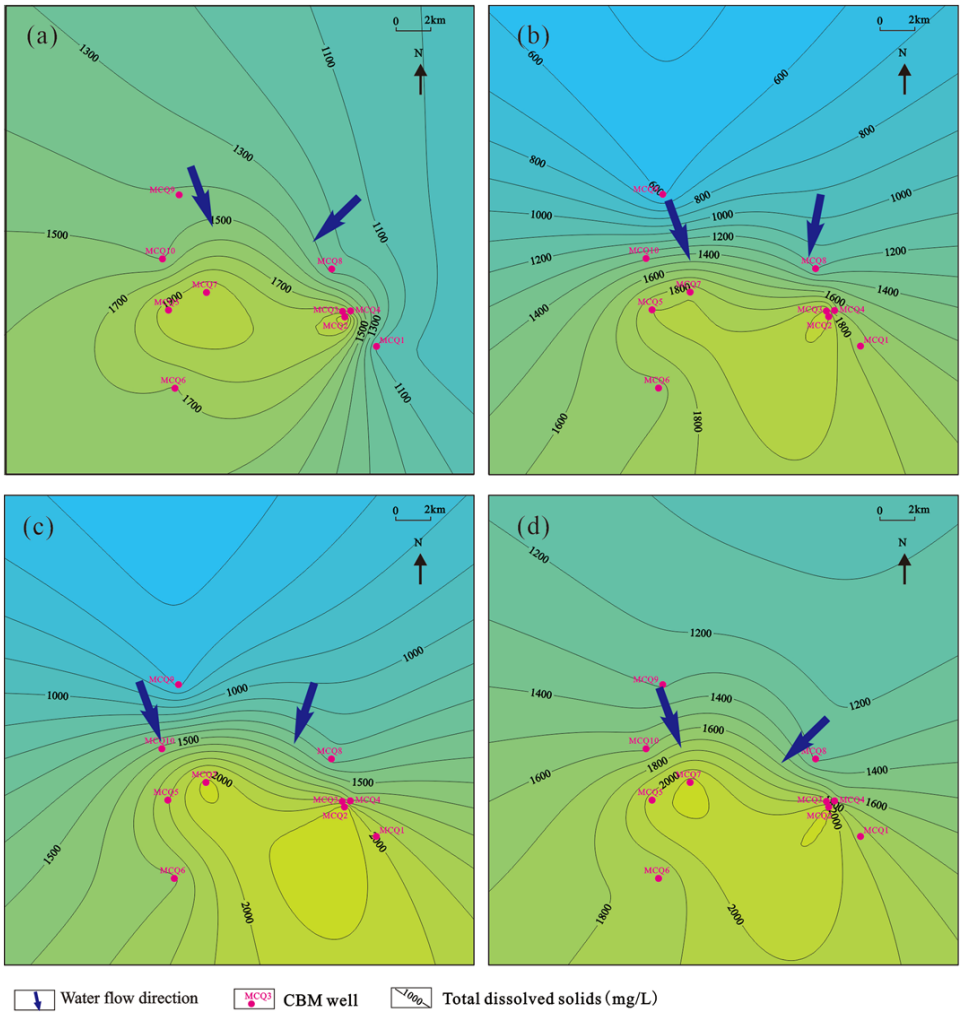


Figure 7. Spatial distribution trends of TDS. ((**a**–**d**) represent the results of the first, second, third, and fourth sampling tests, respectively.)

4.4. Productivity Response

The gas and water production rates at the time of sampling for each well were statistically analyzed (Table 5), and the relationship between production characteristics and ion concentrations at each stage was then analyzed. Due to the limited availability of fifth-round water chemistry samples, the productivity response analysis was restricted to data from the first four sampling rounds.

Table 5. Gas and water production at different sampling times (m^3/d).

Sampling Frequency	1		2		3		4	
Well (MCQ)	**Water**	**Gas**	**Water**	**Gas**	**Water**	**Gas**	**Water**	**Gas**
1	0.95	0	1.04	0	1.04	4	1.04	495
2	1.02	432	1.02	240	1.02	120	1.02	168
3	1.33	624	1.33	0	1.33	216	1.33	360
4	2.79	0	2.79	0	2.79	0	2.79	0
5	/	/	/	/	/	/	/	/
6	0.6	1675	0.6	1301	0.6	485	0.6	477
7	/	1008	/	912	/	744	/	744
8	/	/	/	/	/	/	/	/
9	3.6	251	/	1226	0.36	40	0.55	40
10	0.91	112	1.91	112	0.4	112	0.33	248

"/" indicates no data.

Production data for gas and water, collected across different sampling intervals, clearly indicate that water production was approximately stable in MCQ1, MCQ2, MCQ3, MCQ4, and MCQ6; no water production data are available for MCQ7. Gas production decreased consistently in MCQ2, MCQ6, and MCQ7, remained zero in MCQ4, increased during the latter sampling rounds in MCQ1 and MCQ10, and varied non-monotonically in MCQ3 and MCQ9.

By comparing the relationship between ion concentrations and gas production at different stages (Figure 8), Na^+, HCO_3^-, and TDS all show a trend of initially slow increase followed by rapid increase with increasing gas production. In contrast, Cl^- shows a general decreasing trend with increasing gas production. High-yielding wells are mainly concentrated within certain concentration ranges (HCO_3^- > 1500 mg/L; Na^+ > 500 mg/L; TDS > 1500 mg/L), while Cl^- concentrations in high-yielding wells are generally relatively low. The correlation between K^+ and gas production is not obvious, with high-yielding wells mainly concentrated around 5 mg/L. The enrichment of ions such as HCO_3^- and Na^+ is generally associated with a location far from the recharge zone characterized by oxygen-rich water, representing a closed hydrogeological environment. Such an environment is favorable for coalbed methane enrichment and preservation, and the gas production potential increases [19]. Guo et al. [20] and Liu et al. [21] also found a positive correlation between gas production and TDS.

In the available scatter plots, relatively high gas production values generally occur at lower Ca^{2+}, Mg^{2+}, and SO_4^{2-} concentrations. As the concentrations of these ions increase, gas production tends to decrease. High-yielding wells are mainly characterized by Ca^{2+} and Mg^{2+} concentrations below 5 mg/L, and gas production is extremely low when SO_4^{2-} exceeds 10 mg/L. The enrichment of these three ions can indicate an open hydrogeological environment [19]. In a closed, reducing environment, Ca^{2+} and Mg^{2+} tend to combine with carbonate ions to form minerals such as calcite and dolomite, thereby precipitating out of the water and leading to decreased concentrations. Anoxic, reducing conditions plus sulfate-reducing bacteria trigger desulfidation in groundwater, which may decrease SO_4^{2-} concentrations and increase HCO_3^- concentrations [20]. A productivity response index δ was proposed by Yang et al. [22] based on geochemical indicators to characterize the gas production potential, with the formula as follows:

$$\delta = [\rho(Na^+) + \rho(HCO_3^-)]/[\rho(K^+) + \rho(Cl^-) + \rho(Ca^{2+}) + \rho(Mg^{2+}) + \rho(SO_4^{2-})]$$

where ρ represents the mass concentration of ions.

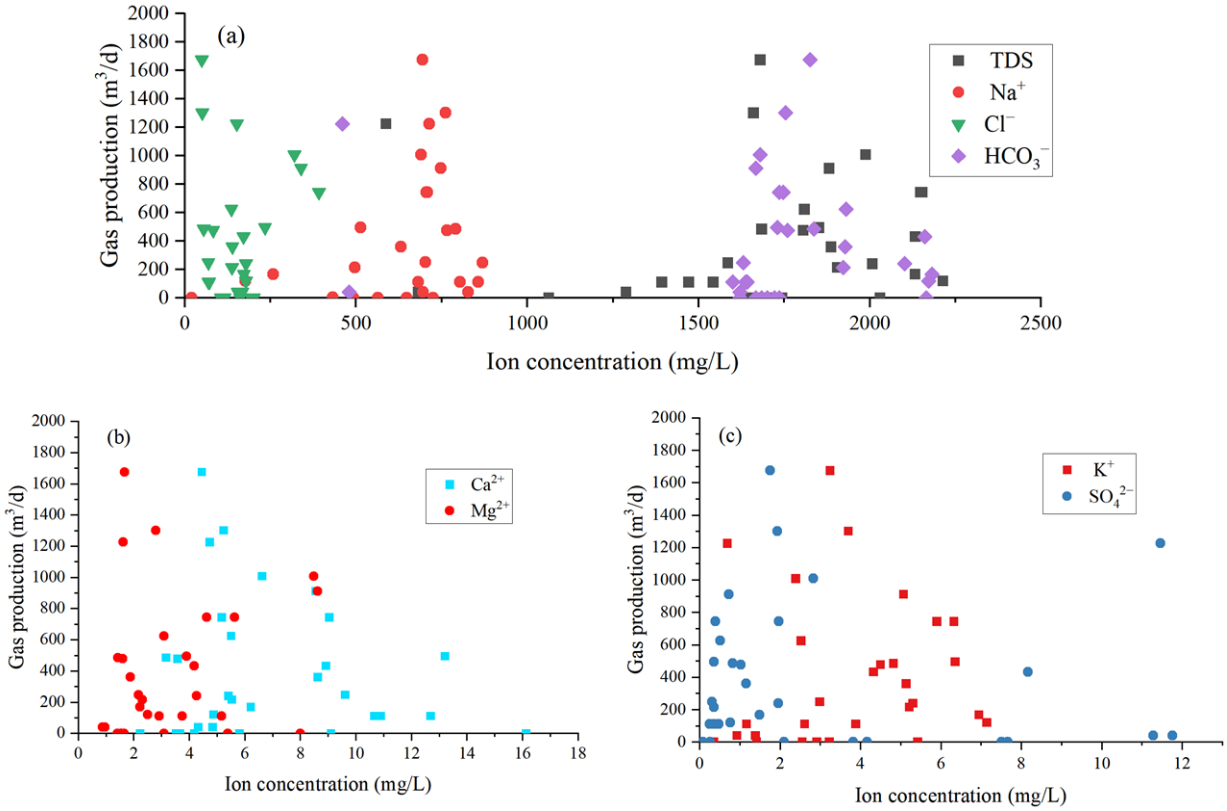


Figure 8. Relationship between ion concentration and gas production. (**a**) TDS, Na^+, Cl^-, and HCO_3^- vs. gas production; (**b**) Ca^{2+} and Mg^{2+} vs. gas production; (**c**) K^+ and SO_4^{2-} vs. gas production.

The δ index was selected because it integrates multiple ions into a single parameter and has been applied in similar CBM settings [22]. This index is used as an exploratory tool for pattern identification rather than a validated predictive model. Its non-monotonic behavior indicates that δ should be interpreted in combination with drainage stage and reservoir conditions. The calculated productivity response index varies from 3.75 to 42.43 across all samples, with an average value of 17.78. As the productivity response index increases, gas production first decreases and then increases (Figure 9). Because Figure 9 combines observations from different wells and drainage stages without distinguishing them, it is unclear whether this pattern reflects temporal evolution within individual wells or differences among wells. In the early stage of drainage, the water preferentially discharged may be "old water" with high TDS but not necessarily the highest relative proportions of Na^+ and HCO_3^-. Cl^-, which becomes enriched in a closed environment, may have a relatively high concentration at this stage, leading to an initial decrease in the δ value, while gas production may not yet have reached its peak. As drainage proceeds, reservoir pressure declines, and effective stress increases rapidly, leading to significant fracture closure and permeability reduction [23,24]. This mechanically induced permeability damage may alter the pathways and rates of water–rock interaction, thereby influencing the concentrations of major ions in produced water. The relative dominance of characteristic ions indicative of a favorable methane enrichment environment (Na^+, HCO_3^-) gradually emerges, while the concentrations of ions representing an open environment (Ca^{2+}, Mg^{2+}, SO_4^{2-}) remain at low levels, causing the δ value to increase. This stage generally corresponds to rising gas production or a period of high and stable production.

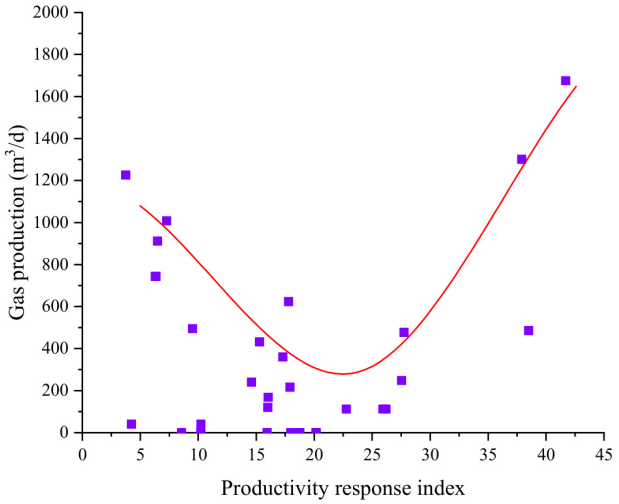


Figure 9. Relationship between productivity response index and gas production.

5. Conclusions

(1) For CBM well produced water in the study area, Ca^{2+}, Na^{+}, K^{+}, and Mg^{2+} serve as the dominant cations, and HCO_3^{-}, Cl^{-}, and SO_4^{2-} as the dominant anions. Na^{+}, Cl^{-}, and HCO_3^{-} show high average concentrations. In contrast, Ca^{2+}, K^{+}, Mg^{2+}, and SO_4^{2-} are low. The TDS of the water comes primarily from Na^{+} and HCO_3^{-}.

(2) Water–rock interactions play a dominant role in shaping the hydrochemical characteristics, as supported by Gibbs diagram analysis, ion ratios, and Br^{-}/Cl^{-} evidence. Wells located closer to the precipitation recharge area yield water that tends to be leachate in character, whereas those farther from the recharge area or in stagnant groundwater zones yield water that tends to be primary sedimentary brine. As drainage proceeds, the concentrations of Na^{+} and K^{+} gradually increase, Ca^{2+} shows a decreasing trend, Cl^{-} gradually increases, and SO_4^{2-} concentration first increases and then decreases. Spatially, TDS increases from north to south, with the central-southern region serving as a stagnant groundwater zone.

(3) Productivity response analysis reveals that Na^{+}, HCO_3^{-}, and TDS all show a trend of initially slow increase followed by rapid increase with increasing gas production. A negative trend is observed between gas production and the concentrations of Cl^{-}, Ca^{2+}, Mg^{2+}, and SO_4^{2-}. The productivity response index (δ) for the Gujiao Block varies from 3.75 to 42.43, with an average of 17.78. However, δ exhibits a non-monotonic relationship with gas production. As the productivity response index increases, gas production initially decreases and then increases.

Author Contributions: Conceptualization, G.W. and Y.Q.; methodology, G.W. and Y.Q.; investigation, G.W. and L.D.; data curation, G.W., Y.Y. and Y.L.; writing—original draft preparation, G.W.; writing—review and editing, G.W.; project administration, G.W. All authors have read and agreed to the published version of the manuscript.

Funding: This research was funded by the Scientific Research Start-up Fund of Shangqiu Normal University (grant number 700140), the Open Fund of the Key Laboratory of Coalbed Methane Resources and Reservoir Formation Process of the Ministry of Education (China University of Mining and Technology) (grant No. 2025-014), and the Natural Science Foundation of Henan Province (grant number 262300421765).

Data Availability Statement: The original contributions presented in this study are included in this article; further inquiries can be directed to the corresponding author.

Conflicts of Interest: Author Liqiang Du was employed by the Shanxi Xi Shan Lan Yan Coalbed Methane Limited Liability Company. The remaining authors declare that the research was conducted in the absence of any commercial or financial relationships that could be construed as a potential conflict of interest. The Shanxi Xi Shan Lan Yan Coalbed Methane Limited Liability Company had no role in the design of this study, in the writing of the manuscript, or in the decision to publish the results.

References

1. Lu, B.J.; Yang, Z.B.; Hou, Y.T.; Li, C.L.; Wang, J.N.; Liu, C.Q.; Yao, Y.H. Desorption-diffusion specificity of deep coalbed methane under high-temperature effects: Implications for development. *Int. J. Min. Sci. Technol.* **2025**, *35*, 1511–1527. [CrossRef]
2. Li, R.T.; Guo, C.; Wang, F. Geochemical characterization and interference determination of produced water in coalbed methane wells of Panhe Block. *Saf. Coal Mines* **2025**, *56*, 45–57.
3. Huang, H.Z.; Bi, C.Q.; Sang, S.X.; Miao, Y.; Zhang, H.J. Signature of coproduced water quality for coalbed methane development. *J. Nat. Gas Sci. Eng.* **2017**, *47*, 34–46. [CrossRef]
4. Wu, Y.; Yin, J.T.; Bai, J.L. Characteristics and Significance of Coalbed Methane Well ProducedWater in Southeast of Ordos Basin. *China Coalbed Methane* **2014**, *11*, 27–30.
5. Xu, L.; Tang, S.; Zhi, Y.; Guo, W.; Liu, T.; Zhang, J. Geological Controls and Geochemical Responses Governing CBM Well Productivity in the Sigong River Block of the Southern Junggar Basin, China. *Processes* **2026**, *14*, 936. [CrossRef]
6. Wang, B.; Xu, F.Y.; Jin, X.; Wang, L.L.; Qu, Z.H.; Zhang, W.S.; Li, Z.; Liu, G.W.; Zhang, Y.T.; Shi, M.J. Evolution of chemical components in produced water from coalbed methane wells in Zhengzhuang block of Qinshui Basin and its response to high productivity. *Acta Pet. Sin.* **2024**, *45*, 1638–1651.
7. Wei, M.M.; Ju, Y.W. Chemical characteristics and origin of produced waters from coalbed gas field in the southern of Qinshui Basin. *J. China Coal Soc.* **2015**, *40*, 629–635.
8. Wang, B.; Xu, F.Y.; Zhang, A.X.; Wang, L.L.; Wang, W.L.; Li, Z.; Qu, Z.H.; Wang, S.; Shi, M.J. Coupling Effect of Water-Rock in the Process of Coalbed Methane Extraction and its Response to Production Capacity-Fanzhuang Block in Qinshui Basin as an Example. *J. China Coal Soc.* **2025**, *50*, 4008–4021.
9. Guo, C.; Gao, J.Z.; Qin, Y.; Yi, T.S.; Chen, Z.L.; Yuan, H.; Wang, G.L.; Lu, L.L.; Li, R.T.; Cheng, X. Geochemical characteristics, genesis, geological and development significance of trace elements in water produced from coalbed methane wells: A case study of Zhijin Block in western Guizhou Province. *J. China Coal Soc.* **2025**, *50*, 3000–3016.
10. Gu, J.Y.; Yang, Z.B.; Tian, W.G.; Han, Y.S.; Liu, C.Q.; Liang, Y.H.; Lu, B.J.; Li, C.L.; Peng, L.S.; Wang, H.C. Geochemical Characteristics and Geological Significance of Produced Water from Coalbed Methane Wells in Junlian, Sichuan. *J. China Coal Soc.* **2025**, *50*, 1647–1658.
11. Jia, D.L.; Wang, H.C.; Tian, J.J.; Xia, D.P.; Wang, B.; Gong, Q.C. Hydrogeochemical characteristics and significance of produced water from coalbed methane wells in Fukang Mining Area. *Saf. Coal Mines* **2025**, *56*, 173–184.
12. Zhou, X.Z.; Wang, S.Q.; Zhu, S.L.; Wang, S.L.; Xiang, G.; Chen, X.H.; Dong, J.H.; Qiu, X. Differences in geochemical characteristics of produced water from coalbed methane wells and their indications for drainage: A case study of the Santang Syncline in Western Guizhou. *Coal Sci. Technol.* **2025**, *53*, 169–182.
13. Wang, G. Coalbed Methane System in the Permo-CarboniferousStrata from Gujiao Block, Shanxi, China. Doctoral Dissertation, China University of Mining and Technology, Xuzhou, China, 2016.
14. Wang, G.; Xie, Y.W.; Chang, H.Z.; Du, L.Q.; Wang, Q.; He, T.; Zhang, S.Y. Characteristics and Geological Impact Factors of Coalbed Methane Production in the Taiyuan Formation of the Gujiao Block. *Processes* **2023**, *11*, 2000. [CrossRef]
15. Zhu, Q.; Yang, Z.G.; Tian, X.H.; Zhao, K. Study on Hydrochemical Characteristics and Formation Mechanism of Shallow Groundwater in the Plain Area South of Beijing and Tianjin. *Geol. Bull. China* **2026**, *45*, 634–646.
16. Gibbs, R.J. Mechanisms controlling world water chemistry. *Science* **1970**, *170*, 1088–1090. [CrossRef] [PubMed]
17. Guo, X.J.; Wang, H.W.; Shi, J.S.; Wang, W. Hydrochemical characteristics and evolution pattern of groundwater system in Baiyangdian wetland, North China Plain. *Acta Geol. Sin.* **2022**, *96*, 656–672.
18. Xu, Y.Q. A Study of the Hydrochemical Characteristics and Geneses of Geothermal Water in the Western Edge of the Sichuan Basin in China. Master's Thesis, China University of Geosciences (Beijing), Beijing, China, 2021.
19. Yang, Z.B.; Wu, C.C.; Zhu, J.P.; Li, Y.Y.; Qin, Z.H. Research Progress on Produced Water Geochemistry from CBM Wells in China. *Coal Sci. Technol.* **2019**, *47*, 110–117.
20. Liu, X.D.; Huang, H.Z.; Li, Z.; Bi, C.Q.; Zhao, Y.K.; Zhang, C. Analysis of Formation Mechanism of Chemical Composition of Drainage Water in Coalbed Methane Wells from Daxing Well Field. *Bull. Sci. Technol.* **2019**, *35*, 11–17.
21. Liu, H.; Luo, Y.; Lei, K.C.; Kong, X.R.; Zhao, L.; Wang, X.H.; Qi, M.H. Hydrochemical characteristics and dynamic evolution of hydrochemical field for the produced water of CBM wells. *Hydrogeol. Eng. Geol.* **2019**, *46*, 92–99.

22. Yang, Z.B.; Wu, C.C.; Zhang, Z.G.; Jin, J.; Zhao, L.Y.; Li, Y.Y. Geochemical significance of CBM produced water: A case study of developed test wells in Songhe block of Guizhou province. *J. China Univ. Min. Technol.* **2017**, *46*, 830–837.
23. Wang, Z.; Xiong, J.; Zhang, Y.; Tao, G.; Pan, J.; Niu, Q. Investigation of Permeability Stress Induced Damage Evolution of Shallow and Deep Coal Reservoirs in the Junggar Basin, China. *Rock. Mech. Rock. Eng.* **2026**, *59*, 5065–5092.
24. Xiong, J.; Wang, Z.; Zhao, Y.; Jin, Y.; Pan, J. Contrasting Stress Sensitivity of Natural vs. Artificially Fractured Deep Coals: Implications for Coalbed Methane Drainage Pressure Control. *Nat. Resour. Res.* **2026**, *35*, 1229–1257.

Disclaimer/Publisher's Note: The statements, opinions and data contained in all publications are solely those of the individual author(s) and contributor(s) and not of MDPI and/or the editor(s). MDPI and/or the editor(s) disclaim responsibility for any injury to people or property resulting from any ideas, methods, instructions or products referred to in the content.